Published in final edited form as:
Biochemistry. 2009 February 10; 48(5): 1016–1024. doi:10.1021/bi802074p.

Role of histidine-86 in the catalytic mechanism of ferredoxin:thioredoxin reductase†

Elizabeth M.Walters‡, **Ricardo Garcia-Serres**§, **Sunil G. Naik**§, **Florence Bourquin**⊥, **Dominique A. Glauser**⊥, **Peter Schürmann**⊥, **Boi Hanh Huynh**§, and **Michael K. Johnson**‡,*
Department of Chemistry and Center for Metalloenzyme Studies, University of Georgia, Athens, GA, 30602, Department of Physics, Emory University, Atlanta, GA, 30322, and Laboratoire de Biologie Moléculaire et Cellulaire, Université de Neuchâtel, CH-2009 Neuchâtel, Switzerland.

Abstract

Ferredoxin:thioredoxin reductase catalyzes the reduction of thioredoxins in plant chloroplasts using the $[Fe_2S_2]$ ferredoxin as a one-electron donor and as such plays a central role in light regulation of oxygenic photosynthesis. The active-site comprises a $[Fe_4S_4]$ cluster next to a redox-active disulfide that is cleaved in sequential one-electron steps and the combination of spectroscopic and crystallographic studies have revealed a catalytic mechanism involving novel site specific cluster chemistry in the oxidized, one-electron and two-electron reduced redox states. Histidine-86 has emerged as a potential proton donor/acceptor in the catalytic mechanism based on redox-related changes in the positioning of the imidazole ring during redox cycling and greatly decreased activity for the H86Y variant. Here we report on spectroscopic and redox characterization of the $[Fe_4S_4]$ center in *Synechocystis* sp. PCC 6803 H86Y ferredoxin:thoredoxin reductase in the accessible redox states of both the as purified and *N*-ethylmaleimide-modified forms, using the combination of UV-visible absorption and variable-temperature magnetic circular dichroism, EPR, resonance Raman and Mössbauer spectroscopies. The results demonstrate that His86 is required for formation of the partially valence-localized $[Fe_4S_4]^{2+}$ cluster that is the hallmark of two-electron reduced intermediate. Taken together with the available structural data, the spectroscopic results indicate a functional role for His86 in protonation/deprotonation of the cluster-interacting thiol and anchoring the cluster interacting thiol in close proximity to the cluster in the two-electron reduced intermediate.

Ferredoxin: thioredoxin reductase (FTR)[1] is the central enzyme of the chloroplast/FTR system, a redox regulatory system that controls the activity of a wide range of oxygenic photosynthesis enzymes in response to light (1-4). FTR transfers the light-generated redox signal received by the chloroplast $[Fe_2S_2]^{2+,+}$ ferredoxin (Fdx) to thioredoxins (Trxs) utilizing a unique active-site consisting of a $[Fe_4S_4]$ cluster and an adjacent redox-active disulfide (5-8). In this manner, FTR converts two light-generated one-electron signals to one two-electron thiol signal which is then transmitted via dithiol/disulfide interchange reactions to specific enzymes which are critical to the regulation of the Calvin cycle. FTR is currently the best characterized example of a unique class of disulfide reductases that utilize novel site-specific reactivity of a $[Fe_4S_4]$ cluster to effect disulfide reduction in two sequential one-electron steps (9-11). Two other examples are currently known. Heterodisulfide reductase, the terminal enzyme of

†This work was supported by grants from the National Institutes of Health (GM62542 to M.K.J. and GM47295 to B.H.H.)

*To whom correspondence should be addressed: telephone 706−542−9378; fax 706−542−9454; e-mail E-mail: johnson@chem.uga.edu.
‡University of Georgia
§Emory University
⊥Université de Neuchâtel

[1]Abbreviations: FTR, ferredoxin:thioredoxin reductase; NEM, *N*-ethylmaleimide; Trx, thioredoxin; Fdx, ferredoxin; WT, wild-type; DTT, dithiothreitol; NHE, normal hydrogen electrode; VTMCD, variable-temperature magnetic circular dichroism.

methanogenic disulfide respiration, utilizes a $[Fe_4S_4]$ cluster that directly interacts with the coenzyme M/coenzyme B heterodisulfide substrate (12;13). Most recently, HypD, a NiFe-hydrogenase maturation protein, was shown to utilize a disulfide redox cascade initiated by a $[Fe_4S_4]$ cluster to cleave a cysteine thiocyanate on HypE in order to facilitate cyanation of the Fe site of the NiFe active site that is assembled on HypC (14). Hence there is considerable interest in understanding the detailed mechanism of $[Fe_4S_4]$ cluster-containing disulfide reductases.

FTR is a heterodimer in the form of a concave disk, 40−50 Å in diameter and measuring only 10Å across at the center. The active site comprises a $[Fe_4S_4]$ cluster and a nearby asymmetrically disposed disulfide and is located close to the center of the disk, with the cluster proximal to the Fdx-binding side and the disulfide proximal to the Trx binding side (11;15). Six conserved cysteines, arranged in three CXC motifs, two CPC ($C^{55}PC^{57}$ and $C^{74}PC^{76}$) motifs and one CHC ($C^{85}HC^{87}$) motif (*Synechocystis* sp. PCC 6803 numbering scheme), are present in the active-site, with Cys55, Cys74, Cys76, and Cys85 ligating the $[Fe_4S_4]$ cluster and Cys57 and Cys87 involve in the redox-active disulfide, see Figure 1. As discussed below, both crystallographic studies (11;15) and spectroscopic approaches (UV-visible absorption and VTMCD, EPR, ENDOR, resonance Raman and Mössbauer) that focus on the properties of the $[Fe_4S_4]$ cluster (6;7;9;10) have been important in developing the two alternative mechanistic proposals summarized in Figure 1. These mechanisms are not necessarily mutually exclusive and each may be operative under different cellular conditions (11).

The oxidized or resting state involves a $S = 0$ $[Fe_4S_4]^{2+}$ cluster adjacent to the asymmetrically disposed disulfide and a weak interaction between the unique Fe site of the cluster and the disulfide sulfur of Cys87 at 3.14 Å is evident in the μ_3-S-Fe-S(Cys55) angle of 129° (3;8) and increased Fe(II) character at the unique Fe site as assessed by Mössbauer spectroscopy (9). Both proposed mechanisms involve sequential one-electron reductions via a one-electron-reduced intermediate in which the disulfide is cleaved and the cluster-interacting thiol, Cys87, ligates at the unique Fe site to yield a novel $S = 1/2$ $[Fe_4S_4]^{3+}$ with five cysteinate ligands as evidenced by crystallographic (11) and spectroscopic (9;10) studies. Spectroscopic studies have shown that three forms of FTR, i.e, *N*-ethylmaleimide-modified FTR (NEM-FTR), a FTR/mutant Trx heterodisulfide complex and the C57S variant, in which the interchange or substrate-interacting thiol, Cys57, has been selectively alkylated with NEM, covalently attached to one of the active-site cysteines of Trx, and mutated to a serine residue, respectively, provide stable analogs of the transient one-electron-reduced intermediate that is observed during enzyme turnover (7;9;10). The mechanistic proposals differ in terms of whether interaction with the Trx substrate to form the heterodisulfide intermediate occurs at the one-electron-reduced or two-electron-reduced level. The viability of the former mechanism is demonstrated by the ability to form one-electron reduced FTR/Trx heterodisulfide complexes with mutant Trxs containing only one of the two active site cysteines (10;11;16) and to reform the active-site disulfide and dissociate Trx on further one-electron reduction (10). The viability of the latter mechanism is demonstrated by the ability of two-electron-reduced FTR to reduce Trx (17) and by spectroscopic and structural studies which show that the Fe-S(Cys87) bond is cleaved in the two-electron reduced form, but that Cys87 remains in close proximity to the cluster leaving Cys57 free to attack the substrate (10;11).

The observation that the two-electron-reduced form of FTR is unique in having an electron-rich $[Fe_4S_4]^{2+}$ cluster with one valence-localized Fe(II)Fe(III) pair, coupled with pH dependent redox properties associated with the one-electron/two-electron redox couple, led to the proposal that Cys87 is protonated and anchored at the cluster by a strong H-bonding interaction to the S of Cys55 (10), see Figure 1. Such an interaction would promote charge build up on the Fe ligated by Cys55 and favor an electron-rich $[Fe_4S_4]^{2+}$ cluster with a valence-localized Fe(II)Fe(III) pair. The recent crystal structure of two-electron reduced FTR shows that Cys87

remains in close proximity to the cluster (11), but suggests that it is deprotonated and stabilized by interaction with the positively charged imidazole ring of His86 which rotates towards the cluster in two-electron reduced FTR and has potential H-bonding interactions with the sulfur atoms of the cluster (3.8 Å) and Cys55 (3.8 Å). However, it is unclear how such an arrangement could induce the novel electronic properties observed for the $[Fe_4S_4]^{2+}$ cluster in the two-electron-reduced form of FTR.

The importance of His86 in the catalytic cycle of FTR is also evident in mutagenesis studies. Replacing His86 with a tyrosine residue dramatically reduces the ability of FTR to activate fructose-1,6-bisphosphatase (only 10% activity versus wild-type), a physiological redox partner of reduced Trx *f*, and also slows down the rate of formation of a heterodisulfide complex with variant forms of Trxs (16). However, the specific catalytic role of His86 has yet to be determined and the effects of the H86Y mutation on the spectroscopic and redox properties of the active-site $[Fe_4S_4]$ cluster have yet to be elucidated. Here we report spectroscopic and redox characterization of the $[Fe_4S_4]$ cluster of *Synechocystis* sp. PCC 6803 H86Y FTR, both in the as-purified and NEM-modified forms of the enzyme, using the combination of UV-visible absorption and VTMCD, EPR, resonance Raman, and Mössbauer spectroscopies. Taken together with the available structural data, the spectroscopic results indicate a direct role for His86 in protonation/deprotonation of the cluster-interacting thiol and anchoring the cluster interacting thiol in close proximity to the cluster in the two-electron reduced intermediate.

MATERIALS AND METHODS

Protein Expression and Purification

The constructions of the overexpression strains, and the procedures used for overexpression and purification of *Synechocystis* sp. PCC 6803 wild-type (WT) and H86Y FTR are described elsewhere (16;18). ^{57}Fe-enriched samples for Mössbauer analysis were obtained by growing cells on ^{57}Fe-enriched LB media prepared by addition of ^{57}Fe ferric ammonium citrate to chelex-resin-treated LB media to a final Fe concentration of 5 mg/L.

Sample Preparation and Handling

Recombinant *Synechocystis* sp. PCC 6803WT and H86Y enzyme were initially purified with varying amounts of the enzyme in a form that closely resembles NEM-FTR based on EPR studies (up to 20% based on EPR spin quantitations). The EPR silent form of recombinant FTR was generally obtained only after redox cycling the enzyme by dithionite reduction followed by O_2 oxidation and is used as the starting material for all studies. NEM-modification of one of the cysteines of the active-site disulfide of WT and H86Y FTR was carried out by reducing FTR with excess reduced methyl viologen, incubating for 30 min to ensure complete reduction of the active site disulfide, cooling on ice for 10 min and treating with a 5-fold excess of NEM for 2 min before quenching the reaction by exposure to air. Excess reagents were removed using a 5 mL desalting column and the samples were concentrated by Amicon ultrafilration with a YM10 membrane. Sample concentrations were based upon $\varepsilon_{410} = 17400\ M^{-1}\ cm^{-1}$ for WT and H86Y FTR (16) and $\varepsilon_{410} = 19500\ M^{-1}\ cm^{-1}$ for WT NEM-FTR and H86Y NEM-FTR (19). Unless otherwise stated, WT and H86Y FTR (both in the as-purified and NEM-modified forms) were in 20 mM triethanolamine hydrochloride buffer, pH 7.3, and sample handling was carried out in a Vacuum Atmospheres glovebox under an Ar atmosphere (<1 ppm O_2).

EPR redox titrations were performed at ambient temperature (25−27 °C) in a Vacuum Atmospheres glovebox under argon (<1 ppm O_2). The pH dependence of the midpoint redox potential was determined using *Synechocystis* sp. PCC 6803 WT or H86Y NEM-FTR in a buffer cocktail containing 200 mM each MES, MOPS, and TAPS buffers which allows for

easy variation of the pH in the desired pH range (6.0−8.5). Mediator dyes were added, each to a final concentration of 50 μM, in order to cover the desired range of redox potentials, i.e., methyl viologen, benzyl viologen, neutral red, safranin, phenosafranin, anthroquinone-1,5-disulfonate, indigodisulfonate, methylene blue, 1,2-napthoquinone, duroquinone, and 1,2-napthoquinone-4-sulfonate. Samples were first oxidized by addition of excess potassium ferricyanide followed by reductive titration with sodium dithionite. After equilibration at the desired potential, a 0.25-mL aliquot was transferred to an EPR tube and immediately frozen in liquid nitrogen. Potentials were measured with a platinum working electrode and a saturated calomel reference electrode and are reported relative to NHE.

Spectroscopic Measurements

UV/visible absorption spectra were recorded on a Shimadzu UV301PC spectrophotometer. Variable-temperature (1.5K − 300K) and variable-field (0 − 6 T) MCD measurements were recorded on samples containing 55% (v/v) poly(ethylene glycol) using an Oxford Instruments SM3 or Spectromag 4000 split-coil superconducting magnet mated to a Jasco J-500C or J715 spectropolarimeter. The experimental protocols used in variable-temperature MCD studies for accurate sample temperature and magnetic field measurement, anaerobic sample handling, and assessment of residual strain in frozen samples have been described in detail elsewhere (20; 21). The MCD intensities are expressed as $\Delta\varepsilon$ ($\varepsilon_{LCP} - \varepsilon_{RCP}$) where ε_{LCP} and ε_{RCP} are the molar extinction coefficients for the absorption of left and right circularly polarized light, respectively. X-band (~9.6 GHz) EPR spectra were recorded on a Bruker ESP300E spectrometer equipped with an ER-4116 dual mode cavity and an Oxford Instruments ESR-9 flow cryostat. Raman spectra were recorded with an Instruments SA U1000 spectrometer fitted with a cooled RCA 31034 photomultiplier tube, using a 457 nm line from Coherent Innova 10-W Ar^+ laser. Scattering was collected at 90° from the surface of a frozen 15 μL droplet of protein in a specially constructed anaerobic cell mounted on the coldfinger of an Air Products Displex model CSA-202E closed cycle refrigerator (22). The spectrum of the frozen buffer solution, normalized to the intensity of the ice-band at 230 cm^{-1} has been subtracted from all the spectra shown in this work. Mössbauer spectra were recorded using the previously described spectrometers (23). The zero velocity refers to the centroid of the room temperature spectra of metallic iron foil. Analysis of the Mössbauer data was performed with the program WMOSS (WEB Research).

RESULTS

The UV-visible absorption spectra of as prepared and dithionite-reduced WT and H86Y FTR and NEM-FTR are shown in Figure 2. Clearly, the H86Y mutation has no significant effect on the absorption properties of either WT or NEM-modified samples. As prepared samples comprise a protein band at 278 nm, a shoulder at 315 nm, and a broad shoulder at 410 nm, and are characteristic of $[Fe_4S_4]^{2+}$ centers (3). The visible absorption properties are not significantly affected by dithionite, indicating that the $[Fe_4S_4]^{2+}$ centers are not reduced by dithionite. In contrast, the as prepared NEM-FTR samples exhibit absorption spectra with pronounced features centered at 330 and 430 nm, in addition to the protein band at 278 nm, that are characteristic of $[Fe_4S_4]^{3+}$ centers (3). Moreover, dithionite reduction of the NEM-modified samples results in absorption spectra indistinguishable from those of as purified samples indicating one-electron reduction to the $[Fe_4S_4]^{2+}$ state (3).

Resonance Raman spectroscopy provides a more discriminating assessment of perturbations in the cluster environment via changes in the frequencies and/or relative intensities of Fe-S stretching modes in the 240−450 cm^{-1} region. Comparisons of the resonance Raman spectra using 457.9 nm excitation of WT and H86Y FTR in as prepared, oxidized NEM-modified and methyl-viologen-reduced forms are shown in Figure 3. The resonance Raman spectra of each

of these forms of WT *Synechocystis* sp. PCC 6803 FTR are all distinct and each has been analyzed in detail in previous studies (6;10). The observation that the resonance Raman spectra of as prepared and oxidized NEM-modified H86Y FTR are indistinguishable from their WT counterparts indicates that H86Y spectra can be interpreted in the same way. Hence, the spectrum of as prepared (oxidized) H86Y FTR is interpreted in terms of an all-cysteinyl-ligated $[Fe_4S_4]^{2+}$ cluster in which one Fe site is weakly interacting with active-site disulfide and the spectrum of oxidized NEM-modified H86Y FTR is interpreted in terms of a $[Fe_4S_4]^{3+}$ cluster with the unique Fe site ligated by two cysteine residues (Cys55 and Cys87) (6;9;10).

Although the H86Y mutation does not significantly perturb the properties of the $[Fe_4S_4]$ clusters in oxidized and NEM-modified forms of FTR, major perturbations in the resonance Raman spectra indicate that it does have a major effect on the cluster properties in the methyl-viologen-reduced forms, as judged by the resonance Raman studies, see Figure 3C. The ability to quantitatively prepare NEM-modified forms of WT and H86Y FTR (see below), attests to the ability of methyl viologen to completely reduce the active-site disulfides in both types of sample (19). The anomalous resonance Raman spectrum of the methyl-viologen-reduced WT FTR sample compared to the as prepared (oxidized) enzyme, i.e. 2−4 cm^{-1} downshifts and inversion of the relative intensities of the two dominant bands corresponding to the symmetric breathing mode of the $[Fe_4S_4]$ core (335 cm^{-1} in methyl-viologen reduced and 337 cm^{-1} in as prepared) and the asymmetric Fe-S(Cys) stretching mode (356 cm^{-1} in methyl-viologen reduced and 360 cm^{-1} in as prepared), has been rationalized in terms of changes in the core structure associated with the formation of an electron-rich $[Fe_4S_4]^{2+}$ cluster with a valence-localized Fe(II)Fe(III) pair as revealed by parallel Mössbauer studies (10). In contrast, the resonance Raman spectrum of methyl-viologen-reduced H86Y FTR is similar to that of the as prepared H86Y FTR which has the active-site disulfide intact and even more closely resembles that of C87A variant in which there can be no interaction of the $[4Fe\text{-}4S]^{2+}$ cluster with the active site disulfide or the free Cys87 thiol (10). Hence resonance Raman data suggest that the two-electron-reduced form of H86Y FTR no longer has an electron-rich $[Fe_4S_4]^{2+}$ cluster with a valence-localized Fe(II)Fe(III) pair. Moreover, the similarity in the resonance Raman properties of as prepared C87A and two-electron-reduced H86Y variants, suggests that the absence of the novel site-specific cluster properties in two-electron-reduced form of H86Y FTR is a consequence of His86 being required to facilitate the interaction of Cys87 with the cluster.

Mössbauer studies of H86Y FTR, see Figure 4, confirm and extend the conclusions of the resonance Raman results, and a comparison of Mössbauer parameters of WT and H86Y *Synechocystis* sp. PCC 6803 FTR is presented in Table 1. The spectra of as prepared and methyl-viologen-reduced H86Y FTR are very similar and are dominated by nearly symmetrical quadrupole doublets, that are readily interpreted in terms of equal intensity overlapping quadrupole doublets from two valence-delocalized Fe(II)Fe(III) pairs with $\delta = 0.44-0.45$ mm/s and $\Delta E_Q = 1.13-1.37$ mm/s. In contrast, as prepared WT FTR has one valence-delocalized pair, $\delta = 0.45$ mm/s and $\Delta E_Q = 1.24$ mm/s, and a partially valence-localized pair with $\delta = 0.54$ mm/s and $\Delta E_Q = 1.84$ mm/s for the more Fe(II) site and $\delta = 0.39$ mm/s and $\Delta E_Q = 1.07$ mm/s for the more Fe(III) site which has been attributed to a weak interaction with the active-site disulfide. Hence the absence of a significant electronic interaction between the disulfide and a unique Fe site of the $[Fe_4S_4]^{2+}$ cluster suggests that the disulfide has moved away from the cluster in the oxidized H86Y variant. The differences in the Mössbauer properties of methyl-viologen-reduced WT and H86Y FTR are much more dramatic. Methyl-viologen-reduced WT FTR has one valence-delocalized pair, $\delta = 0.49$ mm/s and $\Delta E_Q = 1.12$ mm/s, and a valence-localized pair with $\delta = 0.70$ mm/s and $\Delta E_Q = 2.62$ mm/s for the Fe(II) site and $\delta = 0.35$ mm/s and $\Delta E_Q = 1.00$ mm/s for the Fe(III) site. Hence Mössbauer unambiguously demonstrates that the H86Y mutation prevents the interaction(s) that result in the formation of an electron-rich $[Fe_4S_4]^{2+}$ cluster with one valence-localized pair in the two-electron-reduced form of FTR.

The combination of EPR, VTMCD and Mössbauer spectroscopies have all been used to facilitate detailed comparison of electronic and magnetic properties of the $S = 1/2$ $[Fe_4S_4]^{3+}$ centers in the oxidized NEM-modified forms of WT and H86Y FTR. As shown in Figure 5, the EPR spectrum is not significantly perturbed by the H86Y mutation. WT and H86Y samples show almost identical near-axial resonances (g = 2.109, 1.993, 1.982 for WT and g = 2.107, 1.994, 1.980 for H86Y), each accounting for 1.0 spins/FTR and exhibiting analogous spin-relaxation behavior as judged by temperature-dependence studies (3). Hence the ground-state electronic properties of the $[Fe_4S_4]^{3+}$ clusters in NEM-FTR are unaffected by the H86Y mutation. Likewise the excited-state electronic properties are not significantly perturbed as seen by the near coincident VTMCD spectra of the oxidized NEM-modified forms of WT and H86Y FTR (3), see Figure 6. Finally the Mössbauer spectra of the paramagnetic $[Fe_4S_4]^{3+}$ clusters in oxidized NEM-modified forms of WT and H86Y FTR are very similar (cf Figure 4B and Figure 8A of ref (10)) and both can be fit with a similar set of parameters, see Table 1. Hence the valence-delocalization scheme and intracluster magnetic interactions of the $[Fe_4S_4]^{3+}$ cluster in oxidized NEM-FTR are largely unperturbed by the H86Y mutation. Since oxidized NEM-FTR serves as a stable analog of the one-electron-reduced catalytic intermediate (6), these spectroscopic results suggest that His86 is not required for formation of this intermediate.

The possibility that His86 plays a role as a general acid/base in mediating one-electron reduction of NEM-FTR, a stable analog of the one-electron-reduced intermediate, was addressed by investigating the pH dependence of the redox potential of NEM-modified H86Y FTR. Dye-mediated EPR redox titrations were performed at pH 7.0 and 8.0 for the NEM-modified forms of WT and H86Y FTR and the results are shown in Figure 7. In all cases the data are well fit using one-electron Nernst equations and midpoint potentials are reported relative to the normal hydrogen electrode. At pH 7.0, the midpoint potentials for the $[Fe_4S_4]^{3+/2+}$ couple in WT and H86Y NEM-FTR are the same within experimental error, −145 ±10 mV and −155 ±10 mV, respectively. However, at pH 8.0, the physiologically relevant pH for light regulation in chloroplasts, the mutation has a marked effect on the midpoint potential of NEM-FTR, −200 ±10 mV for WT and −275 ±10 mV for H86Y. The changes in the midpoint potential between pH 7.0 and pH 8.0, −55 ±20 mV for WT NEM-FTR and −120 ±20 mV for H86Y NEM-FTR, are indicative of reduction occurring with the addition of one proton for WT NEM-FTR (10) and two protons for H86Y NEM-FTR. More detailed pH dependence studies coupled with parallel structural and spectroscopic studies will clearly be required to fully understand the pH dependence of the midpoint redox potential of both WT and H86Y NEM-FTR. However, the most obvious interpretation is that His86 is responsible for a redox-linked protonation in the one-electron reduction of WT NEM-FTR. In the absence of His86, this one-electron reduction appears to involve addition of two protons, although the nature of the additional redox-linked protonation step observed in WT and H86Y FTR is not known. Hence the redox data implicate a role for His86 in a protonation step associated with the one-electron-reduced/two-electron-reduced redox couple in FTR. The lower redox potential for the one-electron-reduced/two-electron-reduced redox couple in H86Y NEM-FTR at physiological pH may account for the marked decrease in activity associated with H86Y mutation (10% of the wild-type activity).

DISCUSSION

The combination of spectroscopic and structural studies has provided major mechanistic insight concerning the site-specific cluster chemistry that enables the $[Fe_4S_4]$ cluster in FTR to mediate disulfide reduction in two sequential one-electron steps (8-11). Two viable mechanistic proposals have been advanced, based on the characterization of a transient one-electron-reduced intermediate with properties identical to the spectroscopically and structurally characterized oxidized NEM-FTR (7), and the structural and spectroscopic characterization of

catalytically competent intermediates corresponding to two-electron-reduced FTR (17) and one-electron-reduced heterodisulfide complex with a mutant form of Trx containing only one of two active site cysteines (10), see Figure 1. However, the nature and sequence of the protonation/deprotonation steps in the catalytic mechanisms and the question of which of the two proposed catalytic schemes is physiologically relevant or whether both are utilized under different cellular conditions as suggested in Dai et al (11), remain to be determined. In an attempt to address these questions, the spectroscopic consequences of the H86Y mutation have been investigated in this work. His86 is a potential proton donor/acceptor in the catalytic mechanism based on redox-related changes in the positioning of the imidazole ring during redox cycling (11). In addition, since the H86Y mutation results in a marked decrease in catalytic activity (10% of the activity of wild-type) (16), spectroscopic studies that address changes in the properties of the $[Fe_4S_4]$ cluster induced by the H86Y mutation may have the potential to assess the viability of each of the two proposed catalytic cycles.

The results show that the H86Y mutation decreases the weak interaction of the disulfide with the unique Fe site of the $[Fe_4S_4]^{2+}$ cluster in oxidized FTR, but has no significant effect on the spectroscopic properties of the $[Fe_4S_4]^{3+}$ cluster in oxidized NEM-FTR which provides a stable analog of the one-electron-reduced intermediate. By far the most dramatic effect is observed for methyl-viologen reduced FTR which corresponds to the two-electron-reduced intermediate in which the disulfide is cleaved and has been shown to contain a novel electron-rich $[Fe_4S_4]^{2+}$ cluster with one valence-localized and one valence-delocalized Fe(II)Fe(III) pair in WT FTR and a conventional $[Fe_4S_4]^{2+}$ cluster with two valence-delocalized Fe(II)Fe(III) pairs in the H86Y variant. Hence the spectroscopic data demonstrate that His86 is required for the anomalous site specific properties of the $[Fe_4S_4]^{2+}$ center in two-electron-reduced FTR. The effects of the mutation are also evident in a 75 mV decrease in the midpoint potential for one-electron reduction of oxidized NEM-FTR at pH 8, which provides a measure of the one-electron-reduced/two-electron-reduced redox couple in the catalytic cycle. The effect of pH on the redox potentials indicates that this decrease is a consequence of reduction occurring with addition of one proton in WT NEM-FTR compared to two protons in H86Y NEM-FTR, suggesting that His86 itself is responsible for a protonation step in the one-electron-reduced/two-electron-reduced couple in the catalytic cycle of FTR WT.

These spectroscopic and redox results are readily interpreted in light of the active-site structures for the oxidized, oxidized NEM-modified and two-electron-reduced forms of FTR shown in Figure 8 (8;11). In oxidized FTR, the imidazole ring of His86 is not involved in any significant H-bonding interactions and the N atoms of the imidazole ring are positioned away from the cluster and more than 4.5 Å from the S atoms of the active-site disulfide and the N atoms of Arg58 (8). Resonance Raman studies in the Fe-S stretching region show that no significant changes in cluster structure accompany the H86Y mutation. However, Mössbauer studies indicate a decrease in the weak interaction between the disulfide and the unique Fe site (the C87 S-Fe distance is 3.14 Å in WT FTR) occurs in H86Y variant as evidenced by the loss of the partially localized Fe(II)Fe(III) pair, see Table 1. Hence the mutation is likely to position the S of Cys87, and thereby the Cys87/57 disulfide, further from the cluster without altering the overall cluster structure. However, the His86 does not appear to be required for the formation of the novel one-electron-reduced intermediate involving a $[Fe_4S_4]^{3+}$ clusters with two cysteines ligated at the unique Fe site, as judged by UV-visible absorption and VTMCD, EPR and Mössbauer studies of WT and H86Y NEM-FTR which indicate congruent vibrational, electronic and magnetic properties for the clusters in these samples. This is in accord with the structure for oxidized NEM-FTR (11) which shows that the imidazole of His86 is not involved in any significant H-bonding interactions. Although His86 moves closer to the cluster compared to oxidized FTR, the N atoms of the imidazole ring do not interact with the cluster or the coordinating cysteine residues and are more than 4 Å from the S atom of Cys57 and the N atoms of Arg58.

Comparison of the active sites of oxidized and methyl-viologen-reduced forms of FTR (8; 11) reveals that two major structural changes accompany methyl-viologen-induced cleavage of the active-site disulfide, c.f. Figures 8A and 8C. First, in accord with the proposed role as the interchange thiol, Cys57 rotates by 130° away from the cluster and becomes solvent exposed and in a position to attack the substrate disulfide. In contrast, the cluster-interacting thiol, Cys87, remains anchored near the cluster, but not ligated at the unique Fe site. Indeed, the position of the cluster-interacting cysteine, Cys87, is unchanged within experimental error in oxidized and methyl-viologen reduced FTR, with the S---S distance between Cys87 and Cys55 increasing from 3.11 to 3.19 Å and the Fe---S distance increasing from 3.14 to 3.21 Å (8;11). Second, the imidazole ring of His86 flips 120° towards the cluster, bringing the εN of His86 within potential H-bonding range of the S of Cys55 and one of the cluster μ_3-S atoms (both 3.8 Å) (11). The structural data were interpreted in terms of Cys87 being deprotonated and presumably stabilized in close proximity to the cluster by the positively charged imidazole ring of His86 (11). However, several lines of evidence support the alternative explanation in which Cys87 is protonated by His86 and anchored at the cluster by H-bonding to the S of Cys55, as originally proposed based on the spectroscopic properties of the $[Fe_4S_4]^{2+}$ cluster in methyl-viologen reduced FTR (10).

First, the Fe-S(Cys) bond lengths of the coordinating cysteines suggest that the Fe sites ligated by Cys55 (2.48 Å) and Cys85 (2.17 Å) correspond to the Fe(II) and Fe(III) sites of the valence-localized pair, respectively, and that the Fe sites ligated by Cys74 and Cys76 (both 2.31 Å) correspond to the valence-delocalized Fe(II)Fe(III) pair. Hence the assignment of the Fe sites based on the structural data is not consistent with having an additional cysteinate close to the Fe ligated by Cys55 which would stabilize a Fe(III) site rather than a Fe(II) site. In contrast, a strong H-bonding interaction between the thiol form of Cys87 and the coordinated S of Cys55 would promote build up of negative charge at the Fe site creating a valence-localized pair with the unique Fe site corresponding to the Fe(II) component. The lengthening of the Fe-SCys55 bond by 0.10 Å and the shortening of the Fe-SCys85 bond by 0.12 Å, for the $[Fe_4S_4]^{2+}$ cluster in the methyl-viologen reduced state relative to the oxidized state (8;11) is therefore consistent with this interpretation and suggests that the Fe(III) site corresponds to the Fe ligated by Cys85. Second, the dominant H-bonding interaction involving εN of His86 in methyl-viologen reduced FTR is a strong donor H-bond from Arg58 (N---N distance of 2.94 Å) implying that His86 has become deprotonated by proton transfer to Cys87. Third, the pH-dependence of the redox behavior of WT and H86Y oxidized NEM-FTR suggests that His86 is responsible for a protonation step during reduction to the two-electron-reduced state in WT FTR. Although there is currently no structural information for H86Y FTR, the spectroscopic and redox data indicate that Cys87 becomes protonated in the two-electron-reduced form, but is no longer anchored at the cluster by the strong H-bonding interaction, suggesting that His86 functions both as a specific proton donor for Cys87 and in stabilizing the H-bonding interaction with Cys55.

The movement of the imidazole ring of His86 as a result of redox cycling or Trx binding to FTR (11) suggests that His86 functions as a proton shuttle during the catalytic cycle. This work demonstrates that His86 is the proton donor to Cys87 which is released from the cluster after addition of the second electron in both of the proposed mechanisms, see Figure 1. In light of the position of the imidazole of His86 close to the heterodisulfide in the one-electron-reduced FTR/mutant Trx complex (εN ~5 Å from each of the S atoms of the heterodisulfide), it is tempting to speculate that His86 accepts the proton from Cys87 and transfers it to the Trx cysteine involved in the transient two-electron-reduced heterodisulfide intermediate, in order to facilitate Cys87 attack of the heterodisulfide to reform oxidized FTR and release reduced Trx. Our previous redox and chromatographic studies of the one-electron-reduced FTR/C40S Trx heterodisulfide studies demonstrated heterodisulfide cleavage and the formation of unbound oxidized FTR and C40S Trx in a coupled one-electron and one-proton reduction (10). In light of the results presented here, the proton added may be used to reprotonate His86

after it has shuttled the proton from Cys87 to the cysteine of Trx rather than for direct protonation of Trx thiolate.

Unfortunately the results presented herein do not resolve the question of which of the two proposed mechanisms are utilized by FTR. The data presented indicate that both mechanisms would likely be impaired by the H86Y mutation. The two-electron reduced intermediate only occurs when FTR is reduced by two electrons prior interacting with the Trx substrate. Hence the major changes in the two-electron-reduced form that result from the H86Y mutation could account for the marked decrease in catalytic activity based on this mechanistic scheme. However, both catalytic mechanisms involve reduction of a one-electron-reduced form and hence would be adversely affected by the 75-mV decrease in one-electron-reduced/two-electron-reduced couple that accompanies the H86Y mutation, based on the data obtained for NEM-FTR. In addition, the last step in both mechanisms involves disulfide/dithiol exchange leading to reformation of the FTR disulfide and release of reduced Trx. This reaction would be adversely affected by the H86Y mutation for both mechanisms, if His86 mediates proton transfer from Cys87 of FTR to the released cysteine of Trx as proposed above.

Acknowledgment

We thank Dr. Shaodong Dai for keeping us informed of crystallographic studies of ferredoxin:thioredoxin reductase

REFERENCES

1. Schürmann P. Redox signaling in the chlorolasts: the ferredoxin/thioredoxin system. Antioxid. Redox Signal 2003;5:69–78. [PubMed: 12626118]
2. Dai S, Johansson K, Miginac-Maslow M, Schürmann P, Eklund H. Structural basis of redox signaling in photosynthesis: structure and function of ferredoxin:thioredoxin reductase and target enzymes. Photosynth. Res 2004;79:233–248. [PubMed: 16328790]
3. Walters EM, Johnson MK. Ferredoxin:thioredoxin reductase: disulfide reduction catalyzed via novel site-specific [4Fe-4S] cluster chemistry. Photosynth. Res 2004;79:249–264. [PubMed: 16328791]
4. Schürmann P, Buchanan BB. The ferredoxin/thioredoxin system of oxygenic photosynthesis. Antioxid. Redox Signal 2008;10:1235–1274. [PubMed: 18377232]
5. Droux M, Jacquot J-P, Miginac-Maslow M, Gadal P, Huet JC, Crawford NA, Yee BC, Buchanan BB. Ferredoxin:thioredoxin reductase, an iron-sulfur enzyme linking light to enzyme regulation in oxygenic photosynthesis: Purification and properties of the enzyme from C_3, C_4, and cyanobacterial species. Arch. Biochem. Biophys 1987;252:426–439. [PubMed: 3028266]
6. Staples CR, Ameyibor E, Fu W, Gaudet-Salvi L, Stritt-Etter A-L, Schürmann P, Knaff DB, Johnson MK. The function and properties of the iron-sulfur center in spinach ferredoxin:thioredoxin reductase: A new biological role for iron-sulfur clusters. Biochemistry 1996;35:11425–11434. [PubMed: 8784198]
7. Staples CR, Gaymard E, Stritt-Etter A-L, Telser J, Hoffman BM, Schürmann P, Knaff DB, Johnson MK. Role of the [Fe_4S_4] cluster in mediating disulfide reduction in spinach ferredoxin:thioredoxin reductase. Biochemistry 1998;37:4612–4620. [PubMed: 9521781]
8. Dai S, Schwendtmayer C, Schürmann P, Ramaswamy S, Eklund H. Redox signaling in chloroplasts: Cleavage of disulfides by an iron-sulfur cluster. Science 2000;287:655–658. [PubMed: 10649999]
9. Jameson GNL, Walters EM, Manieri W, Schürmann P, Johnson MK, Huynh BH. Spectroscopic evidence for site-specific chemistry at a unique iron site of the [4Fe-4S] cluster in ferredoxin:thioredoxin reductase. J. Am. Chem. Soc 2003;125:1146–1147. [PubMed: 12553798]
10. Walters EM, Garcia-Serres R, Jameson GNL, Glauser DA, Bourquin F, Manieri W, Schürmann P, Huynh BH, Johnson MK. Spectroscopic characterization of site-specific [Fe_4S_4] cluster chemistry in ferredoxin:thioredoxin reductase: Implications for the catalytic mechanism. J. Am. Chem. Soc 2005;127:9612–9624. [PubMed: 15984889]

11. Dai S, Friemann R, Glauser DA, Bourquin F, Manieri W, Schürmann P, Eklund H. Structural snapshots along the reaction pathway of ferredoxinthioredoxin reductase. Nature 2007;448:92–96. [PubMed: 17611542]
12. Duin EC, Madadi-Kahkesh S, Hedderich R, Clay MD, Johnson MK. Heterodisulfide reductase from *Methanothermobacter marburgensis* contains an active-site [4Fe-4S] cluster that is directly involved in mediating heterodisulfide reduction. FEBS Lett 2002;512:263–268. [PubMed: 11852093]
13. Hedderich R, Hamann N, Bennati M. Heterodisulfide reductase from methanogenic archaea: A new catlaytic role for an iron-sulfur cluster. Biol. Chem 2005;386:961–970. [PubMed: 16218868]
14. Watanabe S, Matsumi R, Arai T, Atomi H, Imanaka T, Miki K. Crystal structures of [NiFe] hydrogenase maturation proteins HypC, HypD, and HypE: Insights into cyanation reaction by thiol redox signaling. Molecular Cell 2007;27:29–40. [PubMed: 17612488]
15. Dai S, Schwendtmayer C, Johansson K, Ramaswamy S, Schürmann P, Eklund H. How does light regulate chloroplast enzymes? Structure-function studies of the ferredoxin/thioredoxin system. Quart. Rev. Biophys 2000;33:67–108.
16. Glauser DA, Bourquin F, Manieri W, Schürmann P. Characterization of ferredoxin:thioredoxin reductase modified by site-directed mutagenesis. J. Biol. Chem 2004;279:16662–16669. [PubMed: 14769790]
17. Schürmann P, Stritt-Etter A-L, Li JS. Reduction of ferredoxin:thioredoxin reductase by artificial electron donors. Photosynth. Res 1995;46:309–312.
18. Schürmann P. Ferredoxin-dependent thioredoxin reductase: A unique iron-sulfur protein. Meth. Enzymol 2002;347:403–411. [PubMed: 11898432]
19. Schürmann P, Gardet-Salvi L. Chemical modification of the active site of ferredoxin-thioredoxin reductase. Chimia 1993;47:245–246.
20. Johnson, MK. Variable-temperature magnetic circular dichroism of metalloproteins.. In: Que, L., Jr., editor. Metal clusters in proteins. American Chemical Society; Washington,D.C: 1988. p. 326-342.
21. Thomson AJ, Cheesman MR, George SJ. Variable-temperature magnetic circular dichroism. Meth. Enzymol 1993;226:199–232. [PubMed: 8277866]
22. Drozdzewski PM, Johnson MK. A simple anaerobic cell for low temperature Raman spectroscopy. Appl. Spectrosc 1988;42:1575–1577.
23. Ravi N, Bollinger JM, Huynh BH, Edmondson DE, Stubbe J. Mechanism of assembly of the tyrosyl radical-diiron(III) cofactor of *E. coli* ribonucleotide reductase. 1. Mössbauer characterization of the diferric radical precusor. J. Am. Chem. Soc 1994;116:8007–8014.

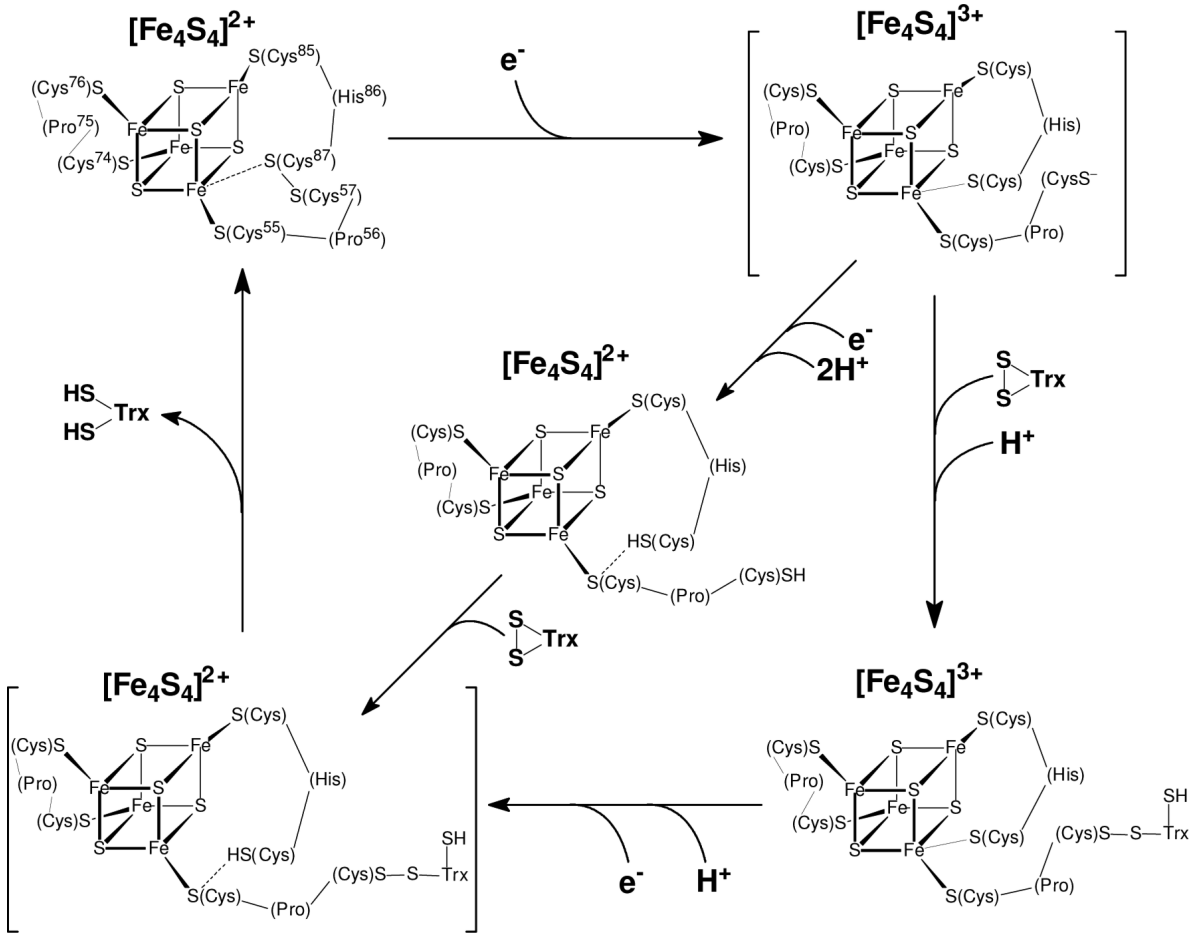

Figure 1.

Proposed catalytic cycles for FTR (10). The mechanisms differ with respect to formation of the heterodisulfide intermediate at the level of the one-electron-reduced or the two-electron-reduced state. Residue numbering is for *Synechocystis* sp. PCC 6803 FTR. Square brackets indicate transient intermediates.

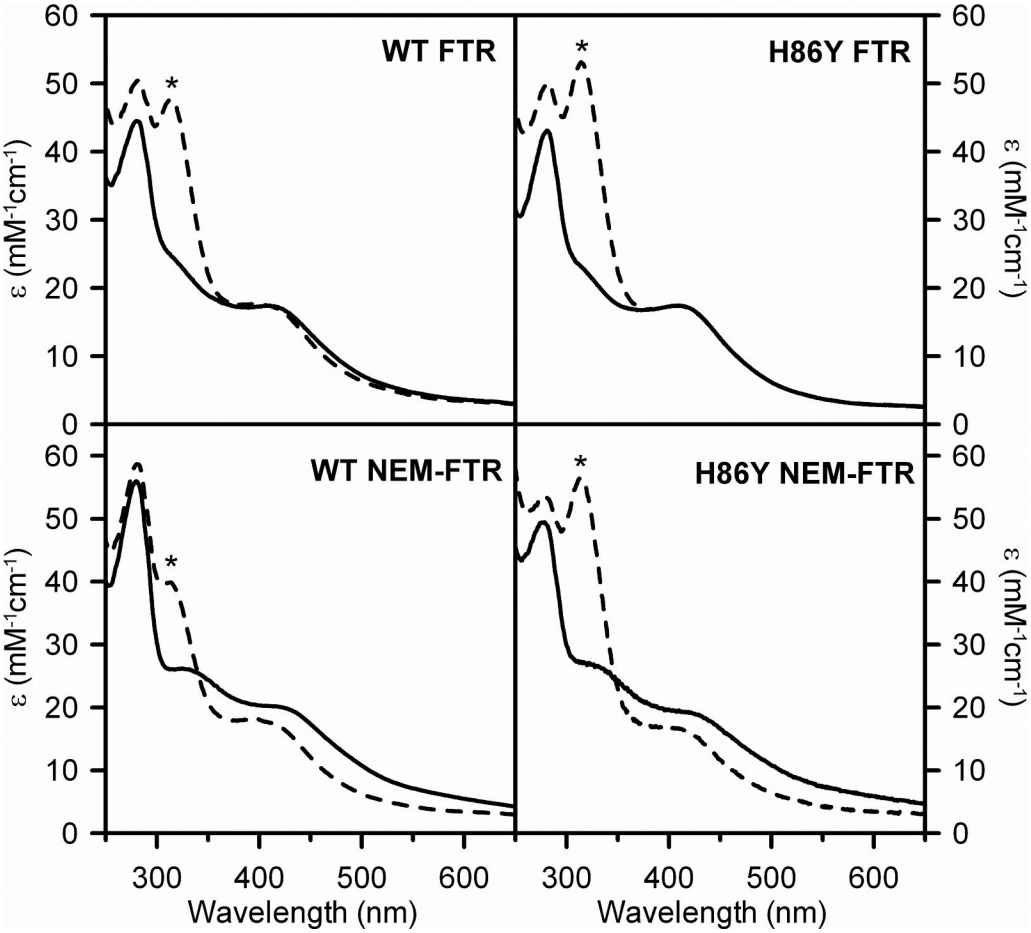

Figure 2.

UV-visible absorption spectra of as prepared and NEM-modified forms of WT and H86Y *Synechocystis* sp. PCC 6803 FTR. In each case, the solid line represents the enzyme as-purified, and the dashed line represents the enzyme anaerobically reduced with excess sodium dithionite. The spectra were recorded in 1-mm cuvettes and protein concentrations were 200 μM (WT FTR), 115 μM (WT NEM-FTR), 303 μM (H86Y FTR), and 60 μM (H86Y NEM-FTR). The bands at 316 nm in the dithionite-reduced samples (marked with an asterisk) originate from excess dithionite.

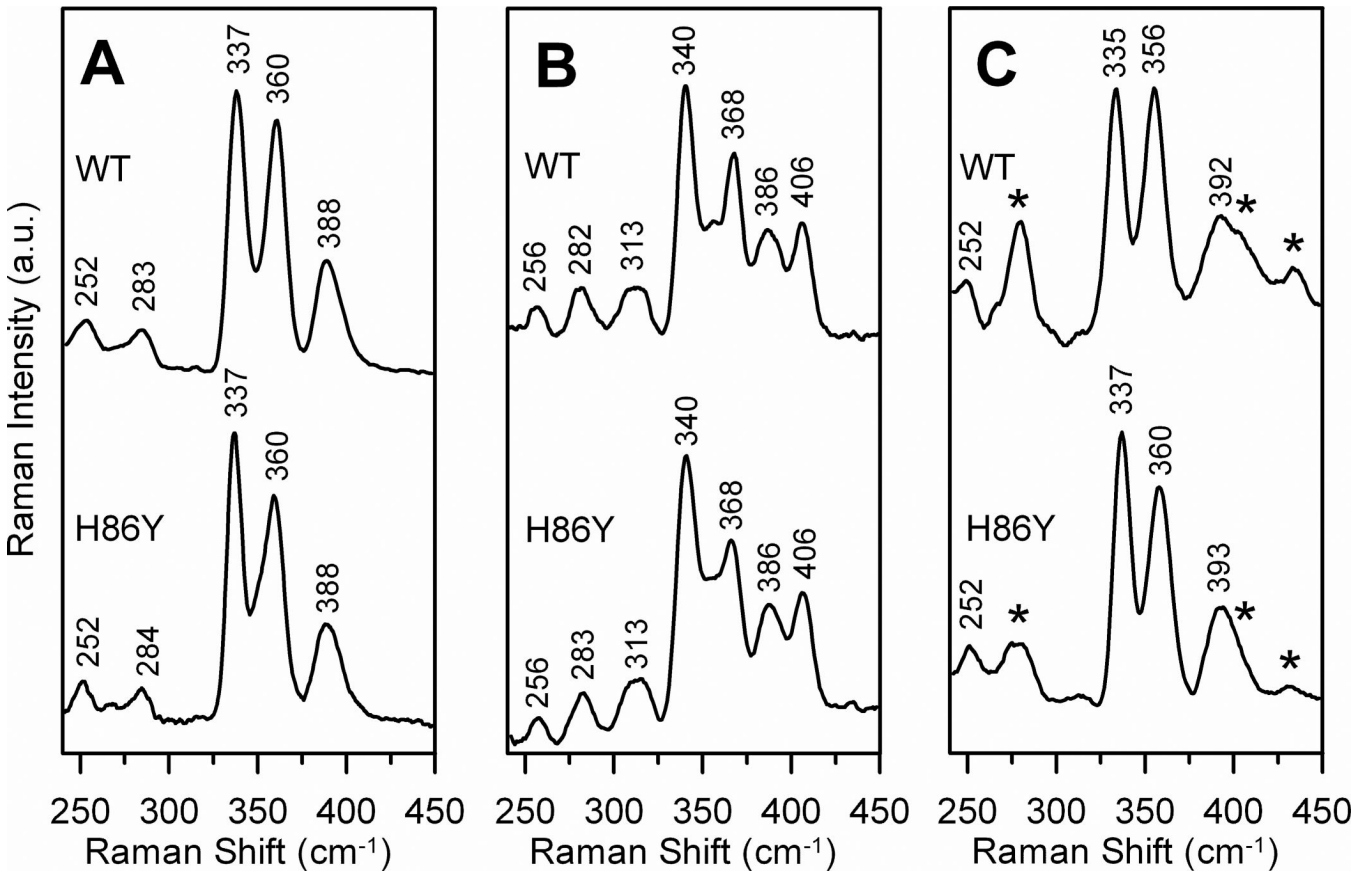

Figure 3.

Comparison of the resonance Raman spectra of WT and H86Y *Synechocystis* sp. PCC 6803 FTR. (A) oxidized (as prepared) enzyme, (B) oxidized NEM-modified enzyme, and (C) methyl-viologen (two-electron) reduced enzyme. All samples were ~3 mM in FTR (except for H86Y NEM-FTR which was ~ 1.0 mM) and all spectra were recorded at 17 K using 457.9-nm laser excitation with ~200 mW laser power at the sample. Each scan involved photon counting for 1 s at 1 cm^{-1} increments with 7 cm^{-1} bandwidth, and each spectrum is the sum of 80−100 scans (except for the spectra of H86Y NEM-FTR which is the sum of 180 scans). For all spectra, the vibrational modes originating from the frozen buffer solution have been subtracted after normalizing the intensities of the “ice-band” at 231 cm^{-1}.

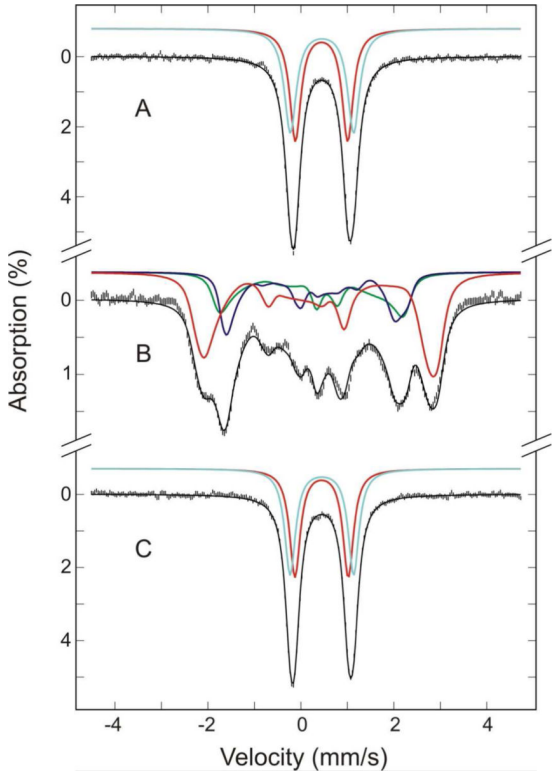

Figure 4.

Mössbauer spectra of *Synechocystis* sp. PCC 6803 H86Y FTR. (A) oxidized (as prepared) FTR, (B) oxidized NEM-modified FTR, and (C) methyl-viologen reduced (two-electron reduced) FTR. The data (hatched marks) were recorded at 4.2 K in a 50 mT magnetic field applied parallel to the γ-beam. The color lines displayed above the experimental spectra are theoretical simulations of the component spectra using the parameters listed in Table 1. Spectra shown in A and C are decomposed into two equal intensity quadrupole doublets (red and cyan lines) representing the two valence-delocalized Fe(II)Fe(III) pairs. Spectrum B is decomposed into three components with an intensity ratio of 1:1:2 representing two Fe^{III} sites, site *a* (blue) and *b* (green), and a valence-delocalized Fe(II)Fe(III) pair (red). The solid black lines overlaid with the experimental spectra are the composite theoretical spectra. For clarity, 2% and 5% contributions of a ferrous impurity have been removed from the raw data of spectra A and C, respectively.

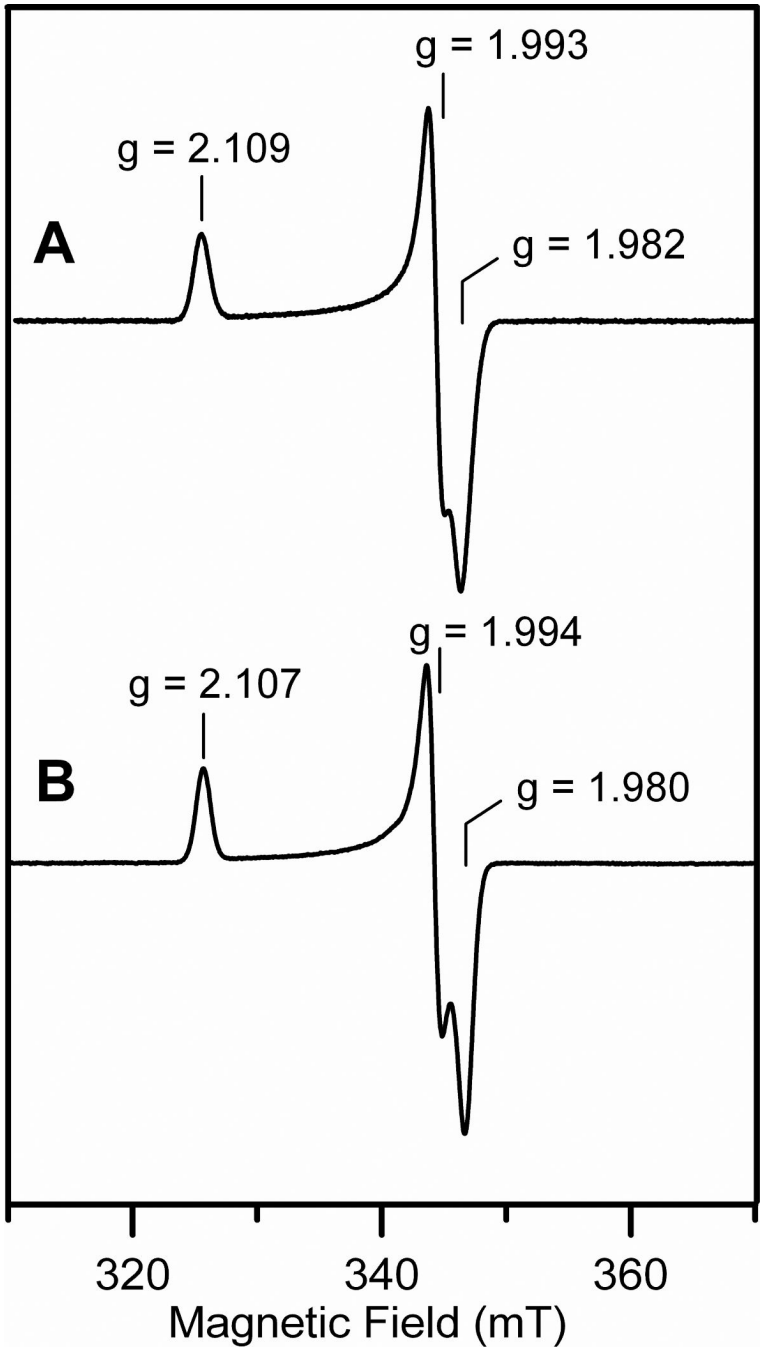

Figure 5.
Comparison of the X-band EPR spectra of the $S = 1/2$ $[4Fe\text{-}4S]^{3+}$ centers in the oxidized NEM-modified forms of WT and H86Y *Synechocystis* sp. PCC 6803 FTR. (A) WT NEM-FTR (185 μM) and (B) H86Y NEM-FTR (150 μM). EPR conditions: temperature, 35 K; microwave power, 1 mW; modulation amplitude, 0.63 mT; microwave frequency, 9.60 GHz.

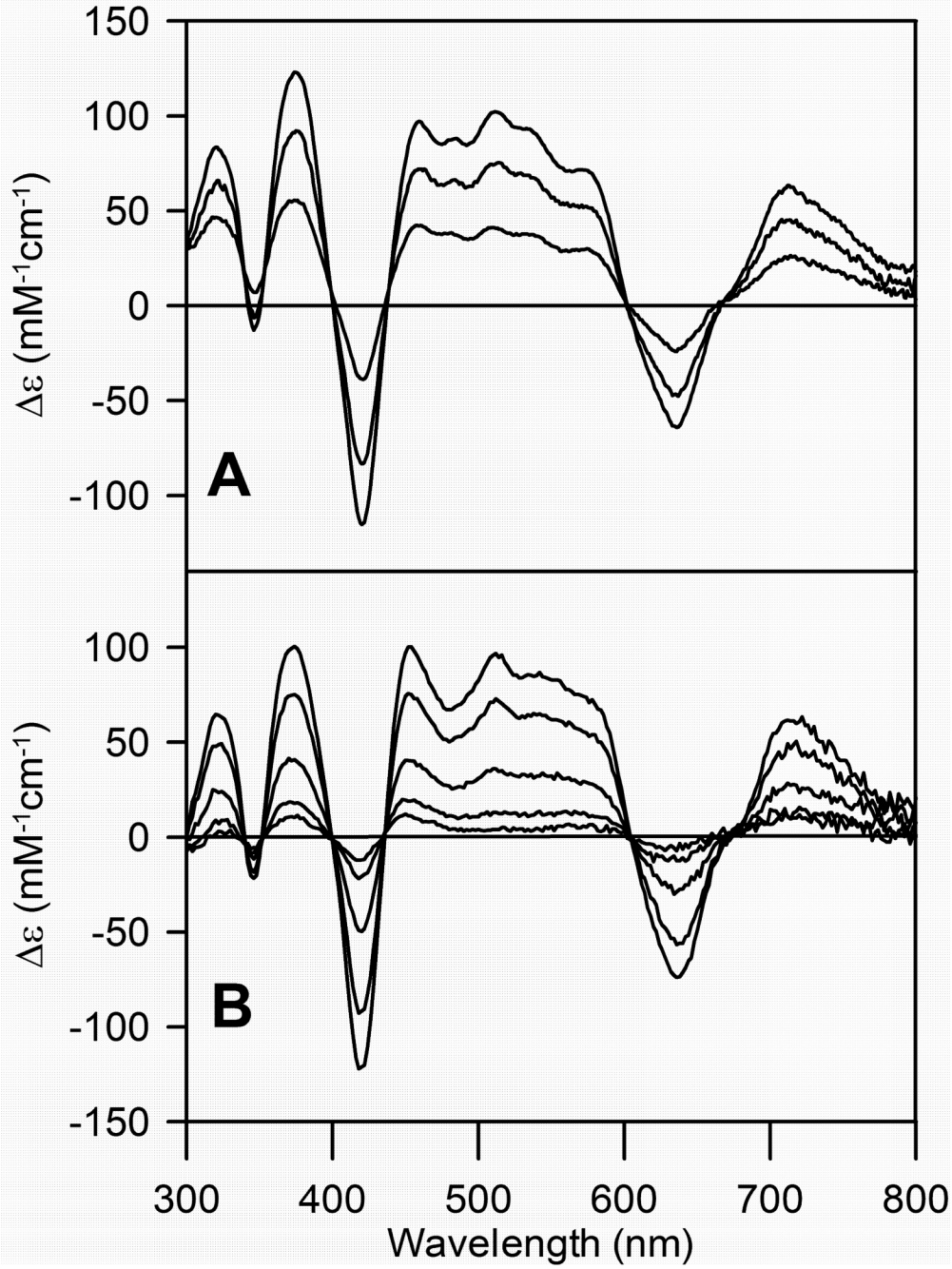

Figure 6.

Comparison of the VTMCD spectra of the $S = 1/2$ $[4Fe\text{-}4S]^{3+}$ centers in the oxidized NEM-modified forms of WT and H86Y *Synechocystis* sp. PCC 6803 FTR. (A) MCD spectra of NEM-FTR collected at 1.68 K, 4.22 K, and 10.4 K, with a magnetic field of 6 T. (B) MCD spectra of H86Y NEM-FTR collected at 1.68 K, 4.22 K. 10.4 K, 25 K, and 50 K, with a magnetic field of 6 T. For all spectra, the intensity of all MCD bands (positive and negative) increase with decreasing temperature.

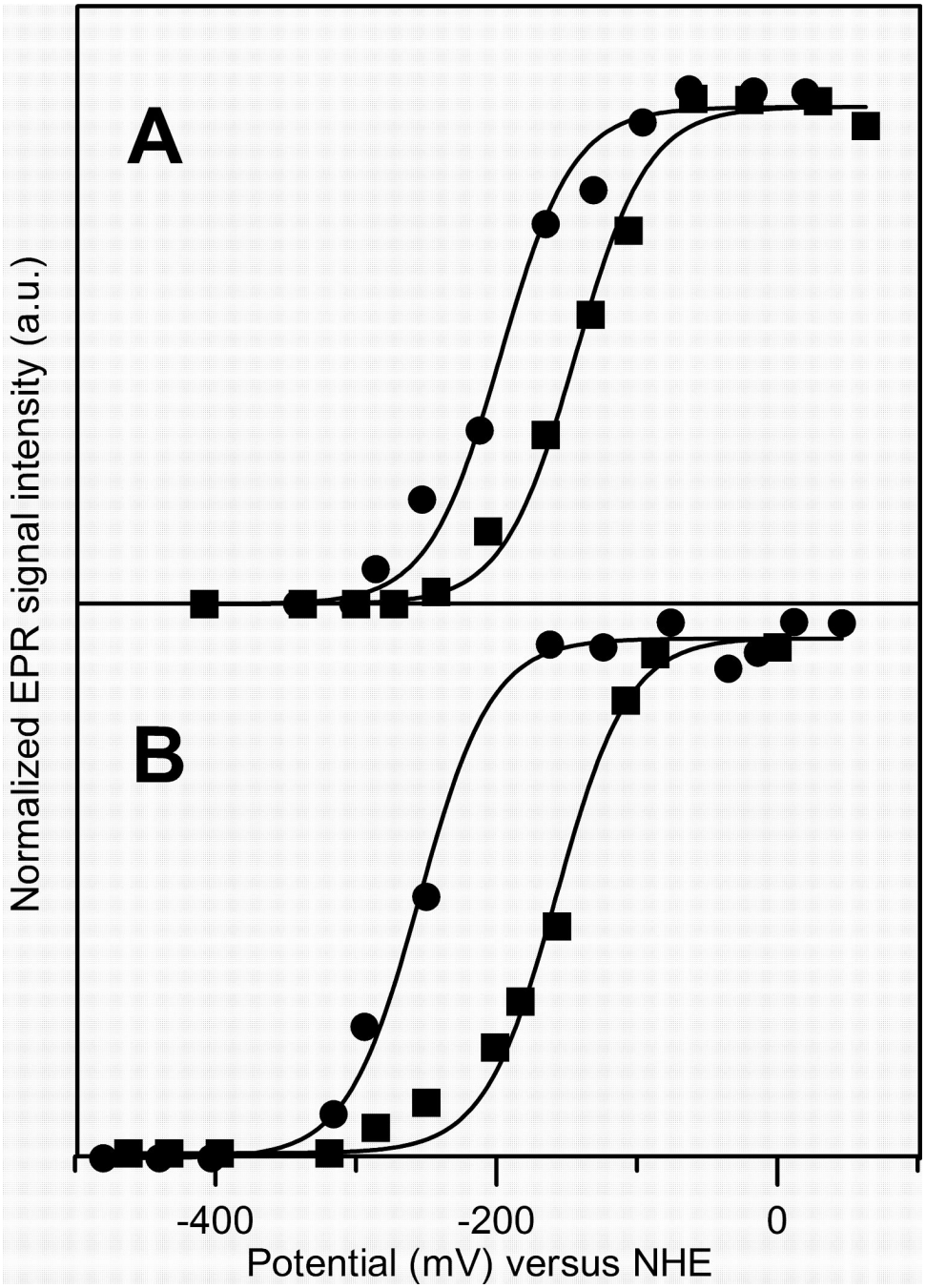

Figure 7.

EPR-monitored redox titrations of WT (A) and H86Y (B) NEM-modified *Synechocystis* sp. PCC 6803 FTR. Data points correspond to the intensity of the $S = 1/2$ EPR from the $[4Fe\text{-}4S]^{3+}$ center at pH 7.0 (■) and pH 8.0 (●). The initial concentration of enzyme used in each titration is 100 μM and all data points have been normalized for dilution effects upon reductive titration with sodium dithionite. The solid lines are the best fits to one-electron Nernst equations with $E_m = -145 \pm 10$ mV (pH 7.0) and -200 ± 10 mV (pH 8.0) for WT NEM-FTR and $E_m = -155 \pm 10$ mV (pH 7.0) and -275 ± 10 mV (pH 8.0) for H86Y NEM-FTR.

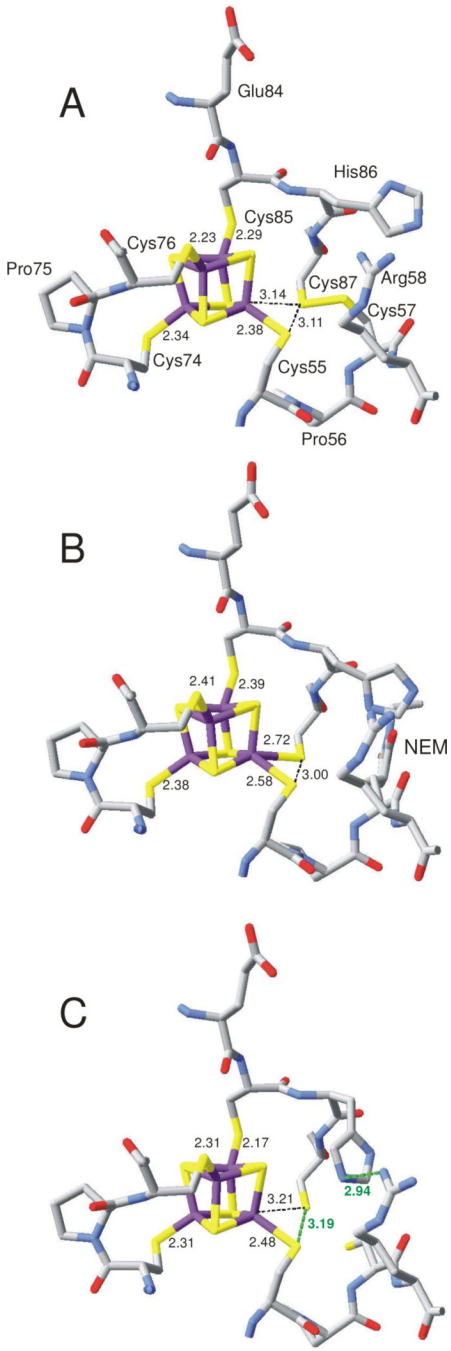

Figure 8.

Active-site structures of *Synechocystis* sp. PCC 6803 FTR: (A) oxidized (as purified) FTR at 1.60-Å resolution (8); (B) oxidized NEM-modified FTR at 1.70-Å resolution (11); (C) methyl-viologen reduced (two-electron reduced) FTR at 1.95-Å resolution (11). Color code: Fe = purple; S = yellow; C = gray; N = blue; O = red. Strong H-bonds are shown as green broken lines with distances in green. Selected Fe-S and S-S distances are indicated in black with broken lines indicating non-bonding or weakly bonding interactions.

Table 1

Comparison of Mössbauer Parameters of WT and H86Y *Synechocystis* sp. PCC 6803 FTR

protein	state	cluster state	Fe site (%)	δ (mm/s)	ΔE_Q (mm/s)	η	$A_{xx}/g_n\beta_n$ (T)	$A_{yy}/g_n\beta_n$ (T)	$A_{zz}/g_n\beta_n$ (T)	Ref
WT	As-purified	$[4Fe\text{-}4S]^{2+}$	a (25%)	0.54	1.84	0.0				(10)
		S = 0	b (25%)	0.39	1.07	0.5				
			c (50%)	0.45	1.24	0.5				
	NEM-modified	$[4Fe\text{-}4S]^{3+}$	a (25%)	0.32	1.2	0.3	20.5	20.5	8.0	
		S = 1/2	b (25%)	0.29	−0.9	0.5	22.0	22.0	19.5	
			c (50%)	0.45	1.2	0.0	−30.0	−25.0	−25.0	
	MV-reduced	$[4Fe\text{-}4S]^{2+}$	a (25%)	0.70	2.62	0.0				
		S = 0	b (25%)	0.35	1.00	0.9				
			c (50%)	0.49	1.12	0.8				
H86Y	As-purified	$[4Fe\text{-}4S]^{2+}$	a & b (50%)	0.45	1.36					This work
		S = 0	c (50%)	0.45	1.13					
	NEM-modified	$[4Fe\text{-}4S]^{3+}$	a (25%)	0.40	0.7	0.0	25.5	23.8	5.0	
		S = 1/2	b (25%)	0.25	−1.0	0.6	23.9	16.3	16.9	
			c (50%)	0.47	1.19	0.0	−26.7	−30.0	−24.1	
	MV-reduced	$[4Fe\text{-}4S]^{2+}$	a & b (50%)	0.45	1.37					
		S = 0	c (50%)	0.44	1.15					